Tuning properties of nanoporous Au-Fe alloys by electrochemically induced surface charge variations

A. K. Mishra,[1,*] C. Bansal,[2] M. Ghafari,[1] R. Kruk,[1] and H. Hahn[1,3]
[1]*Karlsruhe Institute of Technology (KIT), Institute of Nanotechnology, Karlsruhe, Germany*
[2]*School of Physics, University of Hyderabad, Hyderabad, India*
[3]*Technische Universität Darmstadt, Institute of Materials Science, Joint Research Laboratory Nanomaterials, Darmstadt, Germany*
(Received 2 June 2009; revised manuscript received 5 March 2010; published 27 April 2010)

The behavior of strain, magnetization, and resistivity of a nanoporous $Au_{0.55}Fe_{0.45}$ alloy was studied *in situ* during electrochemically induced charge variations on the surface of the alloy. The length of the sample varied reversibly over several cycles of charging and decharging and a maximum fractional length change of 0.14 percent was observed for an induced surface charge of 15 micro-Coulombs/cm^2. The change in magnetization with induced surface charge was dependent on the applied magnetic field and a reversible variation in magnetization of 0.2 percent was observed at the highest applied magnetic field of 6 Tesla. The electrical conductivity could be reversibly changed by 2.5 percent due to the charge induced on the sample. *In situ* Mössbauer spectra recorded during charging and decharging also showed a systematic variation in quadrupole splitting. An attempt is made to explain the observed changes in physical properties quantitatively in terms of the additional charge that is accumulated on the surface of the nanoporous system.

DOI: 10.1103/PhysRevB.81.155452 PACS number(s): 73.63.−b, 75.75.−c, 82.45.Yz

I. INTRODUCTION

In recent years, the possibility of tuning material properties by electrochemical charging has attracted increasing attention.[1–7] The basic idea is that the charge density on the surface of nanoporous materials can be influenced by the presence of charges in the electrolyte during buildup of an electrochemical double layer.[8,9] In nanoporous structures of platinum and gold, reversible changes of strain and electrical conductivity were observed.[1,3,6] In thin films of iron platinum, a reversible change of the coercivity was realized.[7] Charge induced variations in the magnetization of nanoporous Ni-Pd alloys were also observed.[5] In this paper, a study of the tunability of physical properties in a nanoporous Au-Fe alloy is presented. The charge induced variations in strain, magnetization, and electrical conductivity of this alloy system are reported. In an attempt to understand the effects of induced surface charge on the physical properties, the hyperfine interactions were also measured using Mössbauer spectroscopy, which is a good probe for the study of local variations in structure and properties.

II. EXPERIMENTAL DETAILS

Nanoparticles of Au-Fe alloys were prepared using the inert gas condensation technique in a vacuum system pumped initially to a base pressure of 10^{-8} mbar. The set-up of the system used and all experimental details are described in Ref. 8. A gold-iron alloy of nominal composition $Au_{0.5}Fe_{0.5}$, previously prepared by arc melting, was evaporated from a resistively heated crucible. The alloy nanoparticles, produced close to the evaporation source, were transported by a convective gas flow and condensed on a liquid nitrogen filled rotating cylinder. In order to minimize the compositional variation due to the difference in vapor pressure of the constituent elements, the nanoparticles were collected in batches. Subsequently, pellets with diameters of 3 mm were compacted (0.03 GPa) for the *in situ* strain and magnetic measurements. Pellets with rectangular shape ($13 \times 2 \times 0.2$ mm^3) were prepared for the measurements of the electrical conductivity. The microstructure and composition was determined by scanning electron microscopy (SEM) and by energy dispersive x-ray analysis.

Electrochemical charging measurements were performed in a three-electrode configuration with the sample as working electrode (WE), a high-surface area carbon fiber as the counter electrode (CE) and Ag/AgCl as a reference electrode (RE). A solution of 1*M* lithium perchlorate in ethyl acetate was used as the liquid electrolyte. Cyclic voltammograms were recorded using a potentiostat (Autolab). The potential range was restricted to stay within the capacitive double layer region with minimum specific adsorption at the sample. Within the selected region, the potential was scanned repeatedly while simultaneously measuring the physical properties of the sample. Potential scans were performed at rates of 1 mV/sec and 0.5 mV/sec. At each scan rate, several loops were recorded. The initial potential was usually chosen to be in the middle of the potential range. *In situ* dilation measurements were carried out in a Linseis vertical push-rod dilatometer using the cell described in Ref. 1. Magnetic measurements were carried out using a physical property measurement system (PPMS, Quantum Design). Zero-field cooled and field cooled measurements were recorded at an applied field of 200 Oe to determine the temperature of irreversibility. Magnetic isotherms were recorded at temperatures of 10, 60, 70, and 150 K. *In situ* magnetic measurements were carried out in a cell suitable for the small space available in the magnetometer.[5] These measurements were carried out at 275 K while flooding the chamber with helium. The sample was connected as the working electrode and the potential was varied cyclically with respect to the reference electrode. A DC magnetic field was applied while measuring the moment of the sample as a function of time during potential scanning. Simultaneously, the voltammograms were

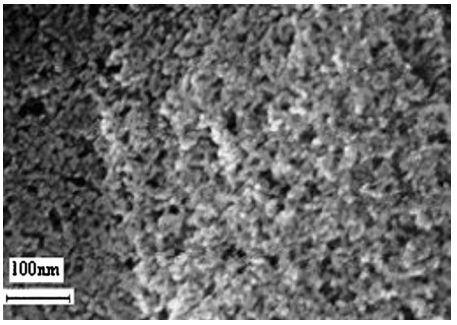

FIG. 1. Scanning electron microscopy image of nanoporous $Au_{0.55}Fe_{0.45}$ alloy.

recorded using the potentiostat. Measurements were carried out at applied magnetic fields of 6, 4, 1, and 0.01 T.

In situ four-probe conductivity measurements were carried out using a cell described earlier.[3] The voltage probes were placed symmetrically at equal distance from the center of the working electrode to avoid any polarization current along each half of the electrode. Cyclic voltammograms were recorded prior to the measurement of the electrical conductivity with the cell filled with electrolyte. The potential was varied with a step width of 0.1 V in the chronoamperometry mode while measuring the resulting current as a function of time. After stabilizing for 300 s at each potential setting, a probe current of 1 mA was applied through the sample and the voltage drop across it was measured. To cancel the effect of any thermo-electromotive force, the voltage drop was measured with the current applied in the reverse direction also. At each potential the charge was calculated by integrating the area under the current versus time curve after correcting for any leakage current.

To observe the local effects of surface charging at the atomic level, Mössbauer spectroscopic measurements were performed *in situ* after electrochemically charging the absorber and holding the charge for the duration of the experiment. This was possible by using the chronoamperometry mode of the potentiosatat. The control potential was applied to the sample and held at a constant value while the spectrum was being recorded. The electrochemical cell was constructed from the thermoplastic material, polyaryletheretherketone (PEEK). The electrolyte compartment of the cell was made from a single block of PEEK. In the central region of the cell an area of 12×12 mm^2 was thinned down to a thickness of 0.2 mm to serve as window for the gamma radiation. A pellet of 13 mm diameter and 20 micron thickness using the nanocrystalline powder was prepared by uniaxial compaction at a pressure of 8 GPa. The mass of the sample was chosen so as to obtain a natural iron concentration of 6 mg Fe/cm^2 in the absorber. The Mössbauer spectra were recorded with counts of approximately 10^6 counts per channel. The spectra were fitted to a quadrupole doublet with a Lorentzian profile for the lines.

III. RESULTS AND DISCUSSIONS

A. Sample characterization

The composition of the powder sample was determined to be $Au_{0.55}Fe_{0.45}$ by energy dispersive x-ray analysis. The specific surface area was determined to be 50(3) m^2/g by the Brunauer-Emmett-Teller (BET) gas adsorption method for the loose powder sample as well as for a pressed pellet. The scanning electron microscopic image in Fig. 1 shows the nanoporous nature of the pellet, which is important for the infiltration of the sample with the electrolyte.

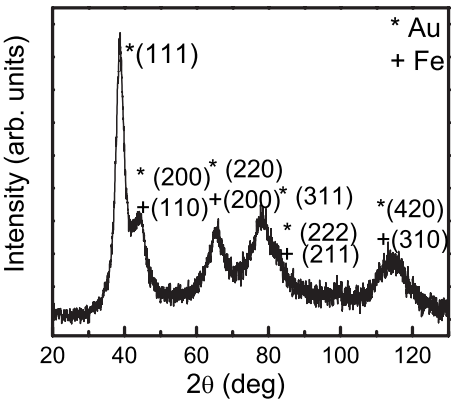

FIG. 2. X-ray diffraction pattern of the nanoporous $Au_{0.55}Fe_{0.45}$ alloy. The overlap of the peak positions of Au and Fe is indicated.

The x-ray diffraction of the nanoporous Au-Fe alloy sample is shown in Fig. 2. After background correction, the diffraction maxima were fitted with Pearson VII function using PROFIT software. The reflections of fcc Au and bcc Fe occur at similar angles and it was not possible to resolve them in the present x-ray diffraction pattern due to the considerable broadening of the line profiles. The x-ray data of AuFe nanoparticles synthesized chemically by a reverse micelle reaction by Cho *et al.* also showed a similar pattern[10] and were interpreted to arise from a core shell structure. The width of the (111) peak, after correcting for instrumental broadening, yielded an average crystallite size of 4(0.5) nm using the analysis of integral breadth of the Bragg reflections.[11,12]

The TEM micrograph is shown in Fig. 3 and the corresponding Iron elemental map using energy filtered transmission electron microscopy (EFTEM) is shown in Fig. 4. The selected area electron diffraction (SAED) pattern also shows the diffraction rings from the Au (111) and higher order

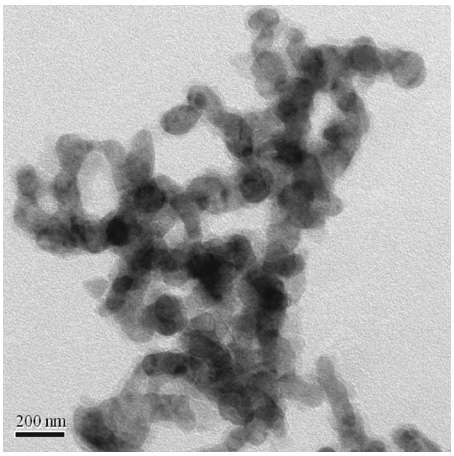

FIG. 3. TEM image of the nanoporous $Au_{0.55}Fe_{0.45}$ alloy.

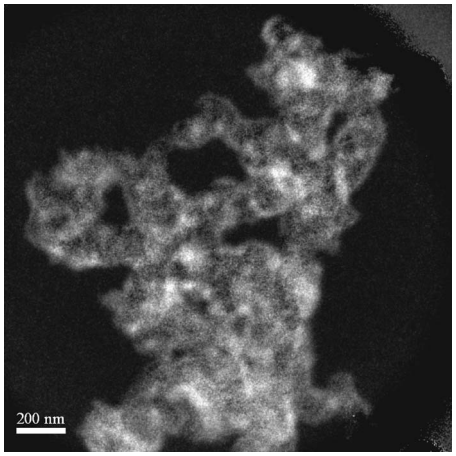

FIG. 4. EFTEM image of the nanoporous $Au_{0.55}Fe_{0.45}$ alloy.

planes, but still the overlap of iron and gold lines could not be resolved. Hence, to get the iron distribution in the sample EFTEM elemental map was taken. The Fe elemental mapping shows that iron is preferentially present in the surface region of the nanostructure. The microstructure of the alloy therefore consists of gold rich core surrounded by an iron rich shell.

B. Dilation measurements

Figure 5 shows the results of the dilatometry measurements during charging and decharging of the sample. In Fig. 5(a), the current is plotted as a function of the applied potential. This plot shows the data of seven consecutive closed potential loops. One can see that the data for all the loops overlap with each other indicating a high reproducibility of

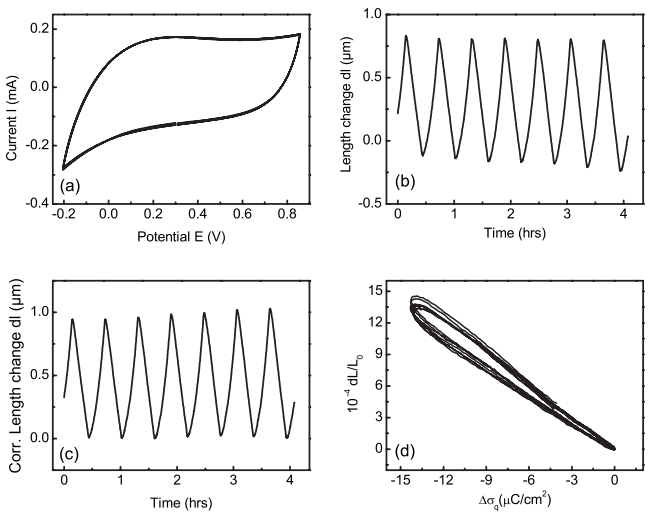

FIG. 5. Results obtained by *in situ* dilation measurements of nanoporous $Au_{0.55}Fe_{0.45}$ alloy. The potential was scanned at a scan rate of 1 mV/sec, and 1*M* $LiClO_4$ in ethyl acetate was used as electrolyte: (a) behavior of current with potential (b) length change as measured in the dilatometer with respect to time (c) corrected plot of length change with respect to time (d) length change with respect to surface charge.

the current during each cycle. The variation of length with respect to time is shown in Fig. 5(b). An irreversible part was also observed which decreased with time. The irreversible part was most likely due to the small shrinkage of the sample by coarsening and sintering at room temperature during the initial cycles. The variation due to this irreversible part was corrected and the resulting curve is shown in Fig. 5(c). From the measured length change of the sample it appears that there is always an increase in length with respect to the initial length of the sample in the potential range for capacitive double layer formation investigated in this work. The length change was zero at the extreme voltage of 0.85 V in the voltammogram and this was taken as the starting point for zero charge on the surface of the sample. In what follows, the charge is surface charge density ($\Delta\sigma_q$) relative to the charge density at 0.85 V has been used. The surface charge density produced on the sample was calculated by dividing the accumulated charge by the total surface area as determined by BET measurements. An overall strain of amplitude ~0.14% was observed for the electrolyte 1*M* $LiClO_4$ in ethyl acetate. Similar measurements were carried out using 0.5*M* lithium per-chlorate dissolved in propylene carbonate (PC).

It was observed that the strain increased with the excess electronic charge on the surface. This trend was observed in both electrolytes employed in the present study. The strain observed with the induced charge in both the electrolytes clearly indicated that it arose effectively from the surface induced charges. Within the selected potential range, any effects due to adsorption can be excluded as seen in the repeating cyclovoltammograms.

In metals, a reversible strain has been reported upon application of surface charges using electrochemical charging.[1] A reversible variation of strain with amplitude of 0.15% was observed in nanoporous platinum. *In situ* measurements of x-ray diffraction indicate a variation of the lattice parameter. In similar experiments on nanoporous gold, a total reversible strain of about 0.2% was obtained.[2] These measurements were explained in terms of the capillary equation and the interface stress[13] produced by the excess surface charges (Lippmann's equation). An equivalent way of looking at the problem is to interpret it in terms of Coulomb forces. The nanostructure of our sample consists of a chainlike interconnected nanoporous structure. On immersion in the electrolyte, a capacitive double layer is produced between the electrolyte and the continuous sample surface. A parallel plate capacitor geometry is attained in the system and a Coulomb pressure is built up on the surface of the nanoporous sample by the Coulomb force.

Fundamental electrostatics[14,15] states that a conductor placed in an electric field will acquire induced charges. The excess charge will be distributed uniformly over the entire surface since the electric field inside a conductor is zero. In the presence of an electric field, the surface charge will experience a force. The force per unit area acting on the surface of the conductor, P_C, always acts outward normal to the surface and is given by

$$P_C = \left(\frac{\sigma_q^2}{2\epsilon}\right)\hat{\mathbf{n}}, \tag{1}$$

where (σ_q) is the surface charge density and $\hat{n}$ is an outward drawn normal. In other words, it can be said that the electric

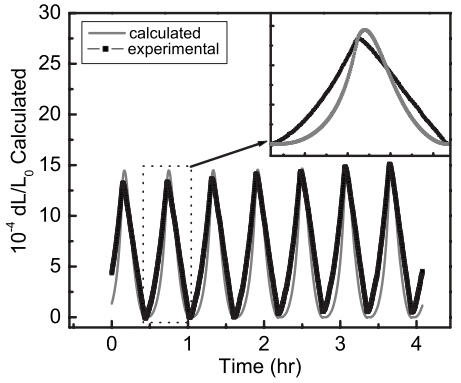

FIG. 6. Comparison of the calculated length change due to Coulombic pressure developed on the surface due to charging and the experimentally observed change in length in $Au_{0.55}Fe_{0.45}$ nanoporous powder immersed in the electrolyte $1M$ $LiClO_4$ in ethyl acetate.

field exerts a negative pressure on the conductor. This implies that due to the induced charge on the surface, the volume of the conductor expands with the increase of pressure. It also suggests that the pressure exerted is independent of the sign of the charge, although a minimum should be observed at the potential of zero charge.

Since, in the selected potential region, the zero strain was observed at maximum applied potential, the change in slope was not observed. Also, the above equation holds for a conductor in vacuum and the dielectric constant of the electrolyte used was not available to us, therefore, it was assumed that the dielectric constant of the electrolyte is equal to that of vacuum. With these two approximations, the pressure developed due to surface charge was first calculated. To estimate the change in volume due to this change in pressure we now use the Bulk modulus viz.

$$B = -V\left(\frac{dP}{dV}\right). \tag{2}$$

Hence, the fractional change in volume is given by,

$$\left(\frac{\Delta V}{V}\right) = \left(\frac{\Delta P}{B}\right). \tag{3}$$

The negative sign is cancelled by the negative sign of ΔP since the pressure is internal. For small strain the volume change was related to the measured length change by using

$$\left(\frac{\Delta V}{V}\right) = 3\left(\frac{\Delta L}{L}\right). \tag{4}$$

Since the experimental value of bulk modulus of Au-Fe alloys was not known, it was approximated using the models available in literature for estimating the bulk modulus of fcc and bcc alloys from values of bulk modulus for end members.[16,17]

Using the estimated value of the bulk modulus for $Au_{0.55}Fe_{0.45}$ alloy $(2.5 \times 10^{11}\ \mathrm{N/m^2})$, the fractional change in length was calculated using Eqs. (1), (3), and (4). Figure 6 compares the experimental and calculated results plotted with respect to time for the sample immersed in the electrolyte $LiClO_4$ in ethyl acetate $(1M)$. The inset of Fig. 6 shows the observed and calculated length change in a small region. A deviation from linearity is evident from this plot which is expected for Eq. (1) which predicts a parabolic dependence of pressure on surface charge density. It shows a reasonable overall agreement. Similar agreement was observed in the other electrolyte used.

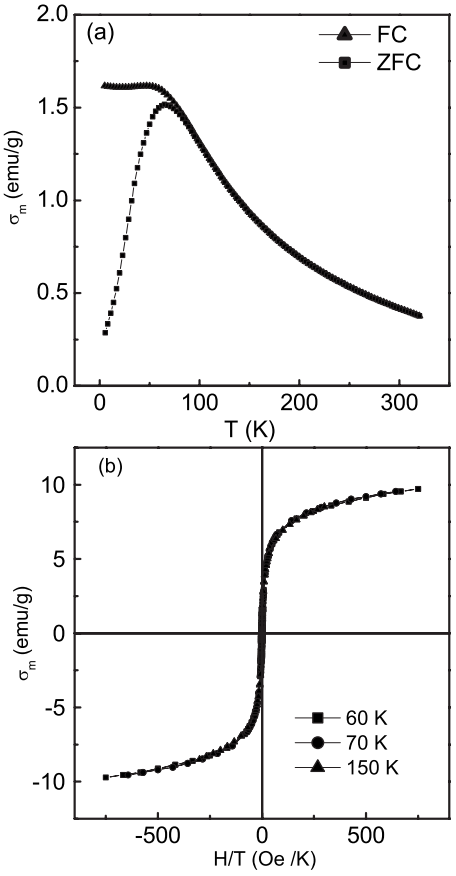

FIG. 7. (a) The temperature dependence of magnetization in the zero field cooled (ZFC) and field cooled (FC) states of nanoporous Au-Fe alloy (b) The magnetization plotted as a function of H/T above the blocking temperature. Both the dependence are characteristic of superparamagnetic behavior of small size particles

C. Magnetic measurements

The temperature and field dependence of magnetization for the nanoporous Au-Fe alloy is shown in Fig. 7. The bulk Au-Fe alloys beyond 17 atomic percent Fe composition are ferromagnetic.[20] However the nanoporous AuFe alloy showed a superparamagnetic behavior with a blocking temperature of 65 K. The coercivity was observed to decrease from 334 Oe at 10 K to zero above the blocking temperature. The magnetization curves superposed when plotted as a function of H/T above the blocking temperature.

Reproducible loops of the variation of magnetization (σ_m) with applied potential during surface charging in the electrochemical cell were observed as shown in Fig. 8. Figures 8(a) and 8(b) show the variation of σ_m with voltage scan at applied fields of 4 and 6 T. It was observed that the magneti-

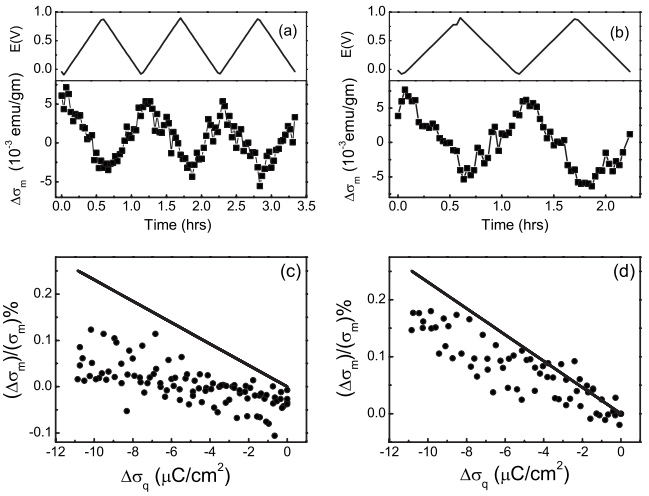

FIG. 8. Reversible variation of mass magnetization by surface induced charging at applied field of (a) 4 T (b) 6 T. The solid lines in the upper parts of (a) and (b) show the variation of the applied potential with time. (c) and (d) shows the variation of fractional change in magnetization with charge. The straight line shows the estimated variations expected from a change in magnetization with surface charge induced pressure.

zation increases with the increase in negative charge on the sample. A change of ~0.2% was observed at an applied field of 6 T. The amplitude of variation was observed to decrease for a lower applied field.

The pressure dependence of saturation magnetization (σ_s) is well known. Using the value of the pressure coefficient of magnetization ($1/\sigma_s$) ($\Delta\sigma_s/\Delta$p) of iron[18] and the bulk modulus of Au-Fe alloy (as estimated earlier), the change in magnetization with the variation in pressure was calculated. Figures 8(c) and 8(d) compare the observed and calculated change in magnetization due to variation in pressure which is built up due to charge on the system. It was observed that at higher fields, the agreement was better as shown in Fig. 8(d). The reason for this is that the expression used for calculation of magnetization with pressure applies to the saturation magnetization, and the sample does not reach complete saturation at lower fields.

D. Conductivity measurement

A fractional variation of ~2.5% in dc electrical conductivity with induced charge was observed as shown in Fig. 9. The effect of Coulombic pressure can account for a variation of only ~0.2% whereas the observed change was much higher. The change in electrical conductivity is therefore an intrinsic effect related to the additional charge on the surface of the metal. According to the simple Drude-Sommerfeld model, the conductivity of a metal depends on the carrier concentration (n) as well as the mean-free path of the carriers (τ) as

$$\sigma = \frac{ne^2\tau}{m}, \tag{5}$$

where e is the electron charge and m is the electron mass, which can be taken to be the free-electron mass for a parabolic s-like band, as is the case here for the 4s conduction band for Au. The observed change in the conductivity can therefore be attributed to an increase in the total charge density in the conduction band and/or a change in the mobility of carriers as a result of change in the scattering by the additional induced surface charge. The variation in fractional conductivity due to charge density deduced from Eq. (6) yields a very simple result,

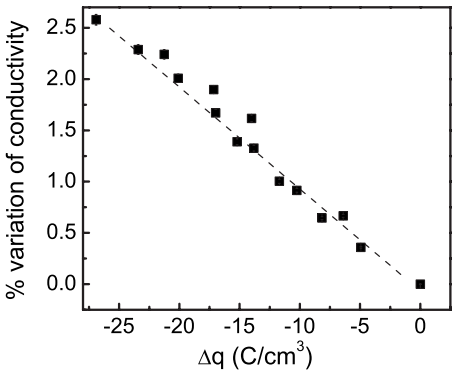

FIG. 9. Percentage variation of relative conductivity with the volume charge for nanoporous $Au_{0.55}Fe_{0.45}$. The slope of the straight line fit gives the charge coefficient of conductivity.

$$\frac{1}{\sigma}\frac{\Delta\sigma}{\Delta(ne)} = -\frac{1}{n|e|}, \tag{6}$$

which depends only on the inverse of the intrinsic carrier concentration. For Au with a free electron concentration of $5.9\times10^{28}/\mathrm{m}^3$ the value of $1/ne$ turns out to be 1.06×10^{-10} m^3/Coulomb. This quantity estimated from the slope of the data given in Fig. 9 has a value 1.03×10^{-9} m^3/Coulomb, which is an order of magnitude higher. This suggests that the additional contribution is arising as a result of the change in carrier mobility which is also expected to change as a result of additional scattering of the carriers by the induced surface charge. The change in mobility of charge carriers has been shown by Dasgupta *et al.*[19] to be the more predominant contribution to the change in conductivity in the indium tin oxide system, where the conductivity changes by several orders of magnitude and a contribution from the change in electron density alone cannot account for the entire effect.

E. Mössbauer spectroscopy

The Mössbauer spectrum of the bulk $Au_{0.5}Fe_{0.5}$ alloy was a magnetic hyperfine field split six line pattern with an average hyperfine magnetic field of 29.5 Tesla and an isomer shift of 0.31 mm/sec relative to alpha iron. This was consistent with the ferromagnetic nature of the sample with a Curie temperature above room temperature as observed in earlier studies on the Au-Fe alloy system.[20] The Mössbauer spectrum of the nanocrystalline powder of $Au_{0.55}Fe_{0.45}$ consisted of a doublet Fig. 10(a) with a quadrupole splitting of 0.80 mm/sec and an isomer shift of 0.35 mm/sec relative to alpha

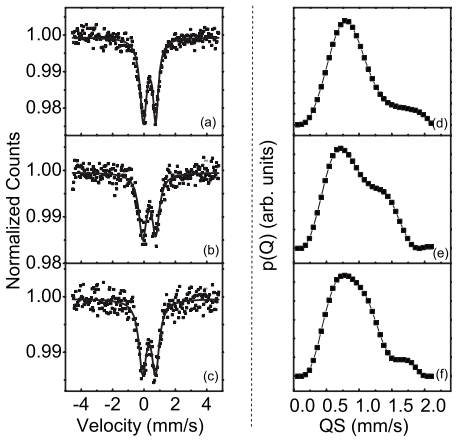

FIG. 10. The Mössbauer spectra obtained during surface charging at various potentials and the respective quadrupole distributions (a) dry sample implies zero charge (b) maximum negative charge (c) return to nearly zero charge (d), (e) and (f) show the corresponding quadrupole distributions.

iron. This was consistent with the superparamagnetic nature of the nanocrystalline powder as also seen in the magnetization behavior.

For *in situ* charging experiments, the Mössbauer spectra were recorded consecutively at various applied potentials. This was done with the potentiostat set in the chronoamperometry mode, wherein the potential was applied at the working electrode (the Mössbauer absorber in our case) and held at that potential and the current through the electrochemical cell was recorded as a function of time. Figure 10 shows the spectra and the quadrupole distributions corresponding to three different states of the Mössbauer absorber. These distributions can be interpreted to give a qualitative information on the atomic level regarding the changes brought about by the charge induced on the surface of the nanomaterial. Figure 10(d) shows the observed quadrupole distribution for the as-prepared dry sample. The main peak in the distribution corresponds to the average value of the quadrupole splitting. The quadrupole distribution for the sample with the maximum possible induced charge is shown in Fig. 10(e). It shows an additional peak at 1.3 mm/sec with about 40 percent area. We can attribute this new peak to the electric filed

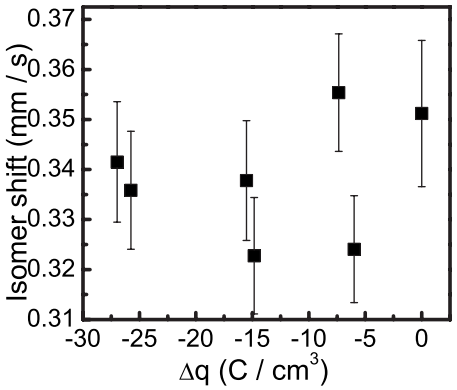

FIG. 11. The variation of isomer shift with induced charge due to electrochemical charging of the Mössbauer absorber.

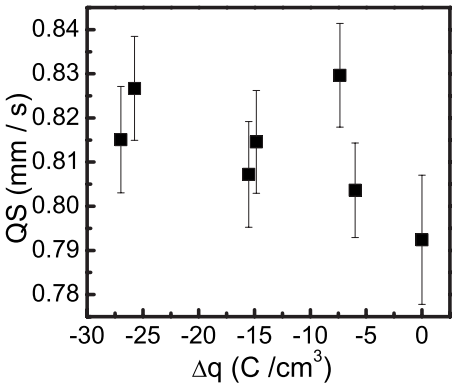

FIG. 12. The variation of average quadrupole splitting as a function of induced charge due to electrochemical charging of the absorber.

gradients seen by the surface atoms because the atoms on the surface will be influenced by the induced charge density as well as the lattice distortions brought about by the induced strain. The quadrupole distribution in Fig. 10(f) corresponds to the case when the sample is in the electrolyte and applied voltage on the electrode corresponds to the lowest induced charge. It was observed that there was a broadened peak due to the overlap of the two peaks indicating that the two peaks have now come closer due to a decrease in the charge.

Figure 11 shows the variation of isomer shifts with charge for the complete potential range of the experiments. The coefficient of pressure dependence of isomer shift of iron in gold is $(-2.1\times10^{-4}$ mm/sec/kbar).[21] The maximum pressure exerted by surface charge as calculated by the strain measurements was about ~11 kbar. This implies a maximum change of 0.0023 mm/sec in isomer shift. The observed shift was about 0.012 mm/sec which is five times higher. This once again brings us to the question whether the entire effect is attributable to a pressure effect alone or there is also a contribution due to the change in electron density of the surface atoms due to electrochemical charging. However, the experimental error bars in the observed isomer shift do not permit us to draw any definitive conclusion. The influence on quadrupole splitting was somewhat more pronounced as seen in Fig. 12. There was clearly an indication from the quadrupole distributions as well as the average values of the quadrupole splitting that the surface atoms experience a local distortion due to the strain induced by the electrochemical charging.

IV. SUMMARY

We investigated the effect of electrochemically induced surface charge on the physical properties of nanoporous gold-iron alloy prepared by inert gas condensation. The observed reversible variation in relative strain with charge was understood to be an electrostatic effect and explained in terms of a Coulombic pressure, which builds up due to surface charge on the nanomaterial.

The effect of surface charging on the magnetization of the alloy was studied at different constant applied magnetic fields. A reversible variation of magnetization with potential

was observed. A relative change of 0.2 percent was observed at high fields. This was explained as an effect of the pressure produced due to induced charge.

Electrical conductivity measurements were carried out in the chronoamperometry mode. A reversible variation in conductivity of about 2.5 percent was observed. The effect was attributed to a change in the charge density in the conduction band, though a small effect due to the change in the mobility of charge carriers was also present.

Mössbauer spectroscopic studies on the $Au_{0.55}Fe_{0.45}$ sample showed a systematic variation in hyperfine interaction parameters with charge. These studies indicated that the influence of the electrochemically induced charges could be evinced at the atomic level also and provided supporting evidence for the changes in the macroscopic physical properties that were brought about by the charge. Two effects of charging, viz. the Coulomb pressure effect due to the surface charge and the concentration effect due the modification of charge density itself, were shown to play a crucial role in the electronically tunable physical properties of nanoporous materials.

ACKNOWLEDGMENTS

The authors would like to thank Torsten Scherer for SEM and EDX measurements and Di Wang for TEM measurements. We are very thankful to J. Weissmüller and C. Lemier for support in the dilatometry and magnetic measurements. The financial support of the DST (India)-DAAD (Germany) project based personnel exchange program and of the Deutsche Forschungsgemeinschaft (DFG) is acknowledged.

*ajay.mishra@int.fzk.de

[1] J. Weissmüller, R. N. Viswanath, D. Kramer, P. Zimmer, R. Würschum, and H. Gleiter, Science **300**, 312 (2003).
[2] D. Kramer, R. N. Viswanath, and J. Weissmüller, Nano Lett. **4**, 793 (2004).
[3] A. K. Mishra, C. Bansal, and H. Hahn, J. Appl. Phys. **103**, 094308 (2008).
[4] C. Bansal, S. Sarkar, A. K. Mishra, T. Abraham, C. Lemier, and H. Hahn, Scr. Mater. **56**, 705 (2007).
[5] C. Lemier, S. Ghosh, R. N. Viswanath, and G. T. Fei, in *Nanoporous and Nanostructured Materials for Catalysis, Sensor, and Gas Separation Applications*, edited by S. W. Lu, H. Hahn, J. Weissmuller, and J. L. Gole, MRS Symposia Proceedings No. 876E (Materials Research Society, Warrendale, PA, 2005), p. R2.6.
[6] M. Sagmeister, U. Brossmann, S. Landgraf, and R. Würschum, Phys. Rev. Lett. **96**, 156601 (2006).
[7] M. Weisheit, S. Fähler, A. Marty, Y. Souche, C. Poinsignon, and D. Givord, Science **315**, 349 (2007).
[8] H. Gleiter, Prog. Mater. Sci. **33**, 223 (1989).
[9] H. Gleiter, J. Weissmüller, O. Wollersheim, and R. Würschum, Acta Mater. **49**, 737 (2001).
[10] S. Cho, A. M. Shahin, G. J. Long, J. E. Davies, K. Liu, F. Grandjean, and S. Kauzlarich, Chem. Mater. **18**, 960 (2006).
[11] H. P. Klug and L. E. Alexander, *X-Ray Diffraction Procedures for Polycrystalline and Amorphous Materials* (Wiley, New York, 1974).
[12] C. E. Krill and R. Birringer, Philos. Mag. A **77**, 621 (1998).
[13] J. Weissmüller and J. W. Cahn, Acta Mater. **45**, 1899 (1997).
[14] J. Griffiths, *Introduction to Electrodynamics*, 2nd ed. (Prentice-Hall of India, New Delhi, 1993).
[15] E. Irodov, *Basic Laws of Electromagnetism* (Mir Publishers, Moscow, 1986).
[16] P. Varotsos, Phys. Status Solidi B **99**, K93 (1980).
[17] K. Giri and G. B. Mitra, Phys. Status Solidi B **134**, K11 (1986).
[18] E. Tatsumoto, H. Fujiwara, H. Tange, and Y. Kato, Phys. Rev. **128**, 2179 (1962).
[19] S. Dasgupta, M. Lukas, K. Dössel, R. Kruk, and H. Hahn, Phys. Rev. B **80**, 085425 (2009).
[20] B. Window, Phys. Rev. B **6**, 2013 (1972).
[21] G. K. Shenoy and E. F. Wagner, *Mössbauer Isomer Shifts* (North-Holland, Amsterdam, 1978).